HHS Public Access

Author manuscript

Chem Res Toxicol. Author manuscript; available in PMC 2020 November 10.

Published in final edited form as:

Chem Res Toxicol. 2019 December 16; 32(12): 2445–2458. doi:10.1021/acs.chemrestox.9b00277.

Impacts of Organomodified Nanoclays and Their Incinerated Byproducts on Bronchial Cell Monolayer Integrity

Todd A. Stueckle[†,§], **Andrew White**[‡,§], **Alixandra Wagner**[‡], **Rakesh K. Gupta**[‡], **Yon Rojanasakul**[‖], **Cerasela Z. Dinu**[*,‡]

[†]Health Effects Laboratory Division, National Institute for Occupational Safety and Health, Morgantown, West Virginia 26505, United States

[‡]Department of Chemical and Biomedical Engineering, Benjamin M. Statler College of Engineering and Mineral Resources

[‖]Department of Pharmaceutical Sciences, School of Pharmacy, West Virginia University, Morgantown, West Virginia 26506, United States

Abstract

Incorporation of engineered nanomaterials (ENMs) into nanocomposites using advanced manufacturing strategies is set to revolutionize diverse technologies. Of these, organomodified nanoclays (ONCs; i.e., smectite clays with different organic coatings) act as nanofillers in applications ranging from automotive to aerospace and biomedical systems. Recent toxicological evaluations increased awareness that exposure to ONC can occur along their entire life cycle, namely, during synthesis, handling, use, manipulation, and disposal. Compared to other ENMs, however, little information exists describing which physicochemical properties contribute to induced health risk. This study conducted high content screening on bronchial epithelial cell monolayers for coupled high-throughput *in vitro* assessment strategies aimed to evaluate acute toxicity of a library of ONCs (all of prevalent use) prior to and after simulated disposal by incineration. Coating-, incineration status-, and time-dependent effects were considered to determine changes in the pulmonary monolayer integrity, cell transepithelial resistance, apoptosis, and cell metabolism. Results showed that after exposure to each ONC at its half-maximal inhibitory concentration (IC_{50}) there is a material-induced toxicity effect with pristine nanoclay, for instance, displaying acute loss of monolayer coverage, resistance, and metabolism, coupled with increased number of apoptotic cells. Conversely, the other three ONCs tested displayed little loss of monolayer integrity; however, they exhibited differential coating-dependent increased

[*]**Corresponding** cerasela-zoica.dinu@mail.wvu.edu. Tel.: +1 304 293 9338. Fax: +1 304 293 4139.

[§]Author Contributions

T.A.S. and A.W.: These authors contributed equally. Co-first authors.

Author Contributions

The manuscript was written through contributions of all authors. All authors have given approval to the final version of the manuscript.

The authors declare no competing financial interest.

ASSOCIATED CONTENT

Supporting Information

The Supporting Information is available free of charge on the ACS Publications website at DOI: 10.1021/acs.chemrestox.9b00277. Chemistry and FTIR spectra of pre- and postincinerated nanoclay coatings; elemental surface analysis of pre- and postincinerated nanoclays; particle hydrodynamic diameter distribution; comparison of hydrodynamic diameters in PBS vs DMEM; single-cell area of ONC-exposed bronchial epithelial cells; particle-only controls for FACS analysis (PDF)

apoptosis and up to 40–45% initial reduction in cell metabolism. Moreover, incinerated byproducts of ONCs exhibited significant loss of monolayer coverage and integrity, increased necrosis, with little evidence of monolayer re-establishment. These findings indicate that characteristics of organic coating type largely determine the mechanism of cytotoxicity and the ability of the monolayer to recover. Use of high content screening coupled with traditional *in vitro* assays proves to serve as a rapid pulmonary toxicity assessment tool to help define prevention by targeted physicochemical material properties design strategies.

Graphical Abstract

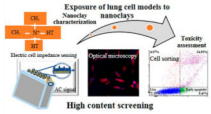

INTRODUCTION

Advanced and additive manufacturing strategies that produce nanocomposites are quickly emerging from research and development into larger scale implementation for industrial, commercial, and healthcare sectors. Reports show that thermoplastic and thermoset nanocomposites, for instance, are rapidly growing at 25% annually and, because of their proven sustainable and low-cost production, are poised to replace older and more costly technologies.[1]

Nanocomposites use one or several engineered nanomaterials (ENMs) incorporated within their matrix to gain such additional technological advantages. One of the largest ENM classes by volume (70%) and the cheapest on a per mass basis for use in nanocomposites fabrication are organomodified nanoclays (ONCs),[2] smectite clays coated with organic modifiers. Because of their large implementation, the ONC industry is projected to be a U.S. $3.3 billion industry by 2023.[3] However, emerging studies showed that ONCs and ONC-derived nanocomposites could harbor health risks along their life cycle.[4–6] The potential for exposure and adverse effects on human health primarily include release of dry particulate during handling, manipulation, use,[5,7] and release during end-of-life disposal or recycling scenarios.[8,9] Studies already reported high airborne concentrations in manufacturing settings with resulting genotoxicity markers in collected blood of exposed workers.[10,11] It is also projected that a majority of end-of-life scenarios for such nanocomposites include municipal incineration and recycling[12–14] and are to lead to similar deleterious health effects. Although less is known about such end-of-life release and subsequent human exposure routes, several controlled studies have appeared to confirm release of airborne particulate during ONC nanocomposite shredding activities for recycling, with silica dust making up the largest proportion of incinerated fly ash.[12,15] Moreover, other recent studies reported that fly ash from incinerated nanocomposite can harbor unique toxicities not present in preincinerated forms.[16–18] In one of such studies it was reported the first dose- and time-dependent pulmonary effects assessment of pre- and postincinerated Cloisite 30B, a quaternary ammonium compound coated nanoclay, to pristine montmorillonite (Cloisite Na) known to induce silicosis-like disease in Fuller’ s Earth miners.[19] Specific results showed that Cloisite

30B induced mild lung airway damage with a delayed low-grade but persistent inflammatory response in aspirated mice, which was overshadowed by a robust, pro-inflammatory response following Cloisite Na exposure. In addition, it was shown that incinerated Cloisite Na with an amorphous pyrogenic silica morphology caused an acute but transient inflammatory response, while incinerated Cloisite 30B, with a more crystalline morphology, produced a low-grade chronic inflammation, similar to crystalline silica.[20] Considering that at present inorganic mineral dust inhalation in occupational settings accounts for 15.4% of asthma and 1.8 million chronic obstructive pulmonary disease (COPD) cases totaling a combined U.S. $6.23 billion[21] and considering that manufacturing sector jobs contribute to 43.8% of silicosis deaths,[22] there is a pressing need to establish toxicity assessment strategies that allow for health risks evaluations along ONCs' life cycle.

The present study aims to establish a high-throughput screening strategy to evaluate potential differences in the toxicity of selected ONCs of prevalent use and their incinerated byproducts, all on a confluent monolayer of human bronchial epithelial cells, a model for human pulmonary airway. To demonstrate the study's feasibility, we hypothesized that the presence of hydroxyl groups in the ONCs would drive a robust and different mode of cytotoxic action on the selected cells when compared to pristine montmorillonite and incinerated byproducts with known surface-available silica groups. Using high content imaging (HCI), electric cell impedance sensing (ECIS), and flow cytometry combined with traditional cell metabolism assay, we foresee the ability to inform and improve "prevention-by-design" strategies to protect workers and general public while retaining the benefits of ONC nanocomposite technology. The generated results are expected to further our understanding of how physical and chemical properties of ONCs along their life cycle influence modes of toxic action to human airways with future investigations in both pulmonary *in vivo* animal models and human workers to be tailored to identify specific adverse health effects, thus proposing strategies that help protect against ONC-induced pulmonary disease.

EXPERIMENTAL PROCEDURES

Nanoclay and Byproduct Sample Information.

Nanoclay samples (i.e., unmodified, bentonite (Nanomer PGV) and surface-modified clays: Nanomer I.31PS (0.5–5 wt % aminopropyltriethoxysilane and 15–35 wt % octadecylamine), I.34TCN (25–30 wt % methyl dihydroxylethyl hydrogenated tallow ammonium), and I.44P (35–45 wt % dimethyl dialkyl amine); Supplementary Figure 1a) were purchased from Sigma-Aldrich. Thermal degradation by incineration of such nanoclays was performed at 900 °C using a TGA701 Thermogravimetric Analyzer (LECO). Briefly, samples were heated at 6 °C/min from 25 to 105 °C in nitrogen to measure the moisture content and at 43 °C/min from 105 to 950 °C to determine the high volatile content. Next, samples were evaluated for ash content at 15 °C/min in O atmosphere and between 550 and 900 °C. Resultant ash was collected and used as a model for thermally degraded byproduct formation (referred to hereafter as PGV900, I31900, I34900, and I44900).[23,24]

Nanoclay and Byproducts Characterization.

The chemical makeup (i.e., surface functional groups) of each nanoclay or resulting byproduct (i.e., nanoclays PGV, I.31PS, I.34TCN, and I.44P and byproducts PGV900, I31900, I34900, and I44900, respectively) was determined by Fourier transform infrared spectroscopy (FTIR) using a Digilab FTS 7000 equipped with a diamond attenuated total reflection (ATR; Varian). Scans were executed at a resolution of 4 cm^{-1} and in a range of 4000–400 cm^{-1}; 100 individual scans were merged and averaged to obtain a full spectrum.

The elemental composition of the individual samples (i.e., nanoclays and byproducts) was evaluated via energy-dispersive X-ray spectroscopy (EDS) on a Hitachi S-4700 Field Emission Scanning Electron Microscope (Hitachi High-Technologies Corp.) operating at 20 kV. Samples were fixed onto carbon tape prior to analysis.

Nanoclays or byproducts size distributions were investigated in phosphate-buffered saline (PBS; Lonza) and Dulbecco's modified Eagle medium (DMEM; Corning) supplemented with 5% fetal bovine serum (FBS; Life Technologies) using dynamic light scattering (DLS) and a Mastersizer 2000 equipped with a Hydro 2000S accessory (Malvern Instruments). For such analysis, solutions of each sample were bath sonicated and added to the Hydro 2000S until laser obscuration was within 10–20%. Measurements were performed at a constant stirring speed of 1750 rpm and under constant sonication with results being presented as the average of 3 consecutive repetitions.

Cell Culture and Treatment.

Low-passage immortalized human bronchial epithelial cells (BEAS-2B; ATCC) were cultured in DMEM supplemented with 5% FBS, 1% L-glutamine (Corning), and 1% penicillin/streptomycin (Life Technologies). Cell cultures were maintained in 100 mm dishes (Corning) and kept in a humidified atmosphere of 37 °C and 5% CO_2. Regular passaging of cells was performed using 0.25% trypsin/ethylene diamine tetraacetic acid (EDTA) solution (Life Technologies).

Half-maximal inhibitory concentration (IC_{50}) values for each nanoclay and its byproduct were determined using BEAS-2B cells seeded at a density of 1.5×10^5 cells/mL into 12-well plates (Thermo Scientific) and following established protocols.[1] Briefly, confluent cells were exposed to nanoclays or byproducts previously bath sonicated for 10 min (2510 Branson, 100 W) in dispersant DMEM supplemented with 5% FBS. The treatment was performed at doses of 0, 0.03, 0.3, 13, 26, 66, 132, and 197 $\mu g/cm^2$ (0–750 $\mu g/mL$) for 24 h. Following exposure, cells were harvested and stained with 0.4% trypan blue solution (Invitrogen). Live cell counts were performed on a Countess automated counter (Invitrogen) to determine IC_{50} values, which were then used in the remaining assays to compare epithelial monolayer integrity and programmed cell death responses.

High Content Imaging.

Cells were seeded into black 96-well high content imaging (HCI) plates (Corning) at a density of 1.5×10^{05} cells/mL and allowed to proliferate and achieve a confluent monolayer for 24 h. The cells were subsequently exposed to the IC_{50} values of each nanoclay or

byproduct (as identified using the strategy listed above) for 24 h. Following exposure, cells were carefully washed with PBS and stained with 1 μL/mL Hoechst 33342 (Thermo Fisher Scientific) and 1 mM CellMask Red (Thermo Fisher Scientific) for 30 min at 37 °C to evaluate and compare monolayer integrity at the different exposure doses.

Stained samples were once again washed with PBS and imaged using the ImageXpress Micro XLS Widefield High Content Analysis System (Molecular Devices) under 10× and 20× objectives. For this the population(s) of cells was analyzed by scanning through the bottom of the plate and acquiring images for each desired fluorescence channel (i.e., chosen to accommodate the above listed staining). Briefly, the blue channel (excitation/emission of 377/447 nm) was used to visualize Hoechst, while the Cy5 (excitation/emission of 628/692 nm) channel was used to visualize CellMask. The experiment was conducted as 3 independent runs with 8 wells per nanoclay or byproduct sample being tested. For each well, 4 independent fields (image size of 1400 × 1400 μm) were sampled.

Accompanying MetaXpress Software v.5.3 was used to analyze each image with the multiwavelenth cell scoring module. Briefly, stained area and mean fluorescence intensity were exported for each cellular event and used to define and analyze cell number, individual cell area, monolayer coverage (percent of stained area with respect to image size), and nuclear distribution (as a function of nuclear area and intensity). For this cells were defined as nuclear (Hoechst positive) events with minimum and maximum widths of 5 and 30 μm as well as an intensity above the local background of 300 gray levels. The module allowed for quantification of single-cell parameters including stained area and intensity. The number of Hoechst-stained nuclei was subsequently used to define cell count, while the mean region of interest (ROI) of Hoechst 33342 was used to define nuclear size. Lastly, single-cell area was defined using the ROI of both wavelengths. Individual cell data was exported to Excel spreadsheets where mean cell area, nuclear area, and nuclear intensity were calculated for each well followed by averaging of replicates. Monolayer coverage was calculated by adding all individual cell areas within an image divided by the image's area and subsequently expressed as mean percentage of stained area with respect to image size.

To eliminate fluorescence-based interference due to dye binding to particulate that inhibits signal (false negative) or results in fluorescent detectable particle (false positive), stained particle only were used as controls and analyzed as indicated above. This analysis identified both size and intensity information for each dye (e.g., small diameter, low or high fluorescent intensity) that was used to screen out the false regions of interest by making adjustments to both the software module's diameter as well as the intensity settings to thus help subtract.

As a supplementary/complementary analysis to the Hoechst/CellMask stain, the assay was repeated by substituting a cytoplasmic stain for a membrane stain. The same exposure conditions and materials were however used. Following exposure, cells were carefully washed with PBS and stained with 1 μL/mL Hoechst 33342 and 5 μM Calcein AM (Thermo Fisher Scientific) for 20 min at 37 °C. Stained samples were again washed with PBS and imaged with a FITC filter (excitation/emission of 470/525 nm) on the ImageXpress system; the same methods of image analysis were applied.

Electric Cell–Substrate Impedance Sensing (ECIS).

Assessment of cellular behavior was performed in real-time with an electric cell impedance sensing instrument (ECIS-Zθ; Applied BioPhysics). For each experiment, a prefabricated ECIS array (96W20idf) of 96 wells (each well containing an electrode) with a total sensing area of 3.985 mm^2 was used. Measurements were performed at a frequency of 4000 Hz. Prior to every cellular experiment the electrodes were stabilized (i.e., to minimize electrode drift) and pre-equilibrated with 200 μL of DMEM for 2 h. After electrode stabilization, BEAS-2B cells were seeded onto the array at a density of 1.5×10^5 cells/mL (22 500 cells/well) in 150 μL of media/well.

Cell cultures were allowed to form a confluent monolayer for 24 h, as determined by a constant resistance instrument reading. After this period they were exposed to the IC_{50} values of the nanoclays or byproducts (as listed above) and monitored continuously for 48 h. Specifically, a multifrequency module was used to monitor the alpha parameter or the resistance due to current passing between the electrode and the basal cell membrane[24–26] and known to be a sensitive indicator of cellular adhesion and cell–substrate interactions.[27,28]

Apoptosis/Necrosis Detection.

The percentages of apoptotic and necrotic cells were determined using a TACS Annexin V-FITC apoptosis detection kit (Trevigen). For this BEAS-2B cells were seeded into 12-well plates at 2.5×10^5 cells/well for 24 h. Cells were then exposed to the IC_{50} values of the nanoclays or byproducts for 24 h, harvested, and centrifuged at 300*g* for 8 min and at 4 °C. Each sample was then incubated with 1 μL of Annexin V-FITC and 10 μL of propidium iodide (PI) prepared in ice-cold 1× binding buffer in the dark at room temperature for 15 min (all reagents were purchased from Invitrogen). Samples were subsequently suspended in 400 μL of binding buffer and analyzed via flow cytometry (LSR Fortessa; BD Biosciences).

FACS excitation of 488 nm and emission wavelengths of 530 (FITC fluorescence) and 610 nm (PI fluorescence) were considered. Approximately 10 000 events were recorded for each sample and scored for percentages of viable (FITC−, PI−), early apoptotic (FITC+, PI−), apoptotic (FITC+, PI+), and necrotic (FITC−, PI+) cells. Analysis was performed using FCS Express 6 software (De Novo Software); double labeling required compensation using cells stained solely with each dye. Additionally, particle-only controls (i.e., nanoclay or byproduct suspended in media) stained with each dye were also analyzed to determine any nanoparticle–dye interactions.

Cellular Viability.

Evaluation of cellular viability upon nanoclay or byproduct exposure was performed using a water-soluble tetrazolium salt (WST-1) assay (TaKaRa Bio). For this cells were seeded into 96-well plates (CELLTREAT Scientific Products) at a density of 1.5×10^5 cells/mL. After 24 h, the cells were treated with the IC_{50} value of each nanoclay or byproduct (identified previously); cells in media served as controls.

Changes in cellular viability were detected as a colorimetric shift resulting from reduction of the tetrazolium salt (4-[3-(4-idophenyl)-2-(4-nitrophenyl)-2*H*-5-tetrazolio]-1,3-benzene disulfonate) into formazan,[29] with the colorimetric change being known to be directly proportional to the quantity of metabolically active cells.[30] Following 24, 48, or 72 h of exposure, 10 μL of WST-1 reagent was added to each well. The cells were incubated for an additional 2 h at 37 °C. Changes in sample absorbance were evaluated using a FLUOstar OPTIMA plate reader (BMG LABTECH) at 485 nm. Media and nanoclay or byproduct suspended in media served as blanks with obtained absorbance measurements from these blanks being deducted from their corresponding cellular measurement(s).

Statistical Analyses.

Each cellular assay was repeated in technical triplicates and biological duplicates ($n = 6$). ECIS was repeated 4 times with biological replicates of 4 for each sample ($n = 16$). All values are presented as the mean value for the indicated replicates with (±) SE bars. Significance was evaluated with a one-way analysis of variance (ANOVA) and the Tukey–Kramer method with JMP 13.0 software (SAS Institute). Results were considered significant when $^*p < 0.05$.

RESULTS AND DISCUSSION

There is a critical need to assess organically modified nanoclays (ONCs) prior to manufacturing, production, use, and disposal in order to design viable strategies that mitigate both user and environmental risks associated with such materials implementation or disposal.[31] The need is driven by large-scale integration of ONCs into both consumer and industrial applications.[3] This study aimed to determine changes in cellular behavior upon exposure to ONCs and pristine nanoclays, all of prevalent use. Using HCI and high-throughput real-time ECIS we proposed overcoming limited metrics and large time scale variations provided by standard single-point cell-based assays such as water-soluble tetrazolium salt (WST-1). By analyzing a large number of cells in complex environments (i.e., upon exposure to pristine nanoclay and ONCs that mimic user manufacturing or their byproducts that mimic disposal by incineration) and by providing numerical representation to characterize induced cellular behavior, we envision the ability to develop a systematic assessment strategy with large applicability and implementation capability to other kinds of nanomaterials or their downstream byproducts, all along their life cycle.

The model systems used for the proposed assessment were selected based on their level of implementation in manufacturing and consumer settings, respectively. Namely, Nanomer clay PGV (pristine bentonite), as well as Nanomer clays I31, I34, and I44 (organically modified bentonites; Figure S1a) have been frequently incorporated into polymer matrices[32–36] and served as test materials to model human inhalation exposure during manufacturing, production, and use. Thermally degraded byproducts of these samples (i.e., PGV900, I31900, I34900, and I44900) served as test materials to model the exposure in a disposal environment by incineration. An immortalized human bronchial epithelial cell line (BEAS-2B) was used for high-throughput cell-based approaches.[37,38]

Physicochemical Characterization of Nanoclays and Byproducts.

The presence of organic modifier was previously shown to influence the toxicity of nanoclays. For instance, Stueckle et al. found that hydrophobic organo-modification resulted in reduced pulmonary toxicity and delayed inflammatory response in mouse lung when compared to exposure to pristine, uncoated nanoclay.[20] We also showed that physicochemical properties such as size, morphology, agglomeration, and surface chemistry of the above selected nanoclays or byproducts alter the behavior of such materials in a biological environment as well as dictate their potential to induce cellular changes.[39,40]

Herein we briefly confirmed previous physicochemical characterization by evaluating pristine nanoclay and ONCs as well as their byproducts. Specifically, with Fourier transform infrared spectroscopy (FTIR) analysis of the as-received clays (Figure S1b) we confirmed the presence of the organic modifiers in all of the ONCs with peaks associated with Si–O–Si (1000 cm^{-1}) and Al–OH-Al (900 cm^{-1}) being identified. We also confirmed that thermal degradation induced loss or shifts of such peaks (Figure S1c), thus indicating loss of both the organo-modifier as well as the aluminosilicate lattice structure.

Analysis of the elemental composition of as-received samples (Figure S2a) revealed that ONCs had higher amounts of C relative to PGV pristine nanoclay. Additionally, I31 and I44 had higher amounts of O and lower amounts of Al, Si, and Fe relative to PGV. These differences in composition further confirmed a previous report and the presence of the organomodifiers in I31, I34, and I44.[23] Thermal degradation caused a decrease in C and increase in O, Al, and Si content, thus confirming loss of both the organic modifiers and the aluminosilicate lattice structure (Figure S2b). Lastly, our analysis of the hydrodynamic particle size in different inert and cell culture media (Phosphate Buffer Saline-PBS and Dulbecco's modified Eagle medium-DMEM, respectively) showed that I31 and I34 had smaller sizes (submicrometer range) in DMEM when compared to pristine nanoclay PGV or I44 (Table S1 and Figure S3). These size differences were likely due to nanoclay– or nanoclay coating–medium interactions, leading to such events as protein corona formation[41] and particle repulsion, respectively,[42] namely, hydrophilic PGV and hydrophobic I44 were more likely to strongly associate with their respective hydrophilic and -phobic regions of proteins present in the DMEM medium. On the other hand, I31 and I34, which have relative intermediate hydrophobicity compared to PGV and I44, would have had induced less protein adsorption to yield better dispersion.[43,44] Furthermore, their respective modifiers containing amine (I31) and hydroxyl (I34) groups induced varied dispersity via hydrogen bonding, van der Waals forces, and electrostatic interactions and caused clay repulsion.[42]

Following thermal degradation, no differences in size distribution were observed for the byproducts, further confirming loss of the organic modifier and ability for the previously listed interactions (Table S1).

High Content Imaging (HCI) at Half-Maximum Inhibitory Concentration (IC_{50}).

The HCI approach was next employed to study biological indicators of cytotoxicity as resulted from exposure to pristine nanoclay, ONCs, and their byproducts, namely, monolayer integrity, cellular size, and nuclear distribution. For this a confluent monolayer of BEAS-2B

that mimicked pulmonary function was considered to accurately predict lung injury/response. It is known that cell–cell adhesion as well as monolayer formation are integral factors in epithelial cell differentiation.[45] Previous reports showed that monolayer formation regulates growth, spreading, migration, proliferation, viability, and cytoskeletal function of cells.[46–48] BEAS-2B cells were considered suitable models[49] since previous research showed that they could serve as an accurate *in vitro* system for evaluating lung-related toxicity.[50]

The fixed dose considered for the HCI analysis was from previously reported IC_{50} values for each of the nanoclays or byproduct being used in this study.[23] Briefly, the reported IC_{50} was obtained upon exposure of BEAS-2B cells to a range of different sample concentrations (0–197 $\mu m/cm^2$); dose range was chosen to mimic exposure in manufacturing/disposal environments[51] and represent a working lifetime exposure of 45 years based on 8 h/day and 50 weeks/year while accounting for particle and lung characteristics.[52] Analysis showed that resulting IC_{50} values for the nanoclays and their byproducts were 85.4 $\mu m/cm^2$ for PGV, 5.25 $\mu m/cm^2$ for I31, 2.63 $\mu m/cm^2$ for I34, 13.1 $\mu m/cm^2$ for I44, 105.1 $\mu m/cm^2$ for PGV900, 39.4 $\mu m/cm^2$ for I31900, 52.5 $\mu m/cm^2$ for I34900, and 46.0 $\mu m/cm^2$ for I44900.[23]

HCI analyses showed that cells exposed to PGV (Figure 1) had a significant loss of monolayer coverage (up to 6.4%) when compared to unexposed controls (Figure 2a). Such significant loss of monolayer coverage was mirrored in cell nuclear counts (Figure 2b). Further, there were changes in the individual cell shape, such as cell elongation, as well as observed loss of membrane integrity (Figure 1, white arrows). Changes in PGV-exposed cellular morphology from their typical oval nature (shown for controls) to a more stretched, spindle-shaped profile could potentially indicate cell survival and initiation of wound healing response, such as EMT.[53]

Relative to controls, cells exposed to I31, I34, and I44 (Figure 1) exhibited no significant changes in their monolayer coverage (87%, 91%, and 77.2%, respectively; Figure 2a). On the contrary, cells exposed to PGV900, I31900, I34900, and I44900 (Figure 1) showed a significant loss of monolayer coverage (about 55%, 40%, 55%, and 32%, respectively-Figure 2a). Moreover, cells exposed to PGV900 showed a significantly higher monolayer coverage relative to cells exposed to PGV, while cells exposed to I31900, I34900, and I44900, respectively, exhibited significantly lower monolayer coverage than their as-received ONC counterparts. No significant changes to single-cell area were detected upon treatment with nanoclays and byproducts, all with respect to the controls (Figure S4).

Analysis of the nuclear area of cells exposed to ONCs and byproducts relative to controls (Figure 2c) showed that there was a significant loss for cells treated with PGV (average of 38.1 μm^2) relative to control cells (average of 219.5 μm^2). Moreover, cells exposed to I44900 showed a significant 9% loss in nuclear area (from 219.5 to 198.8 μm^2). However, cells treated with I31, I34, and I44 and their byproduct counterparts did not exhibit significant changes when compared to the controls. Lastly, analysis of nuclear intensity (Figure 2d) revealed a significant loss for cells exposed to PGV (59%) relative to control cells. Yet, cells treated with I31, I34, and I44 exhibited no significant changes when compared to controls (i.e., 13%, 7%, and 7%, respectively). Cells exposed to PGV900 also

did not exhibit significant change in nuclear intensity (14%) relative to controls, while exposure to I31900, I34900, and I44900 caused significantly higher nuclear intensities (i.e., 32%, 24%, and 29%, respectively) than control values. Furthermore, it was noted that cells exposed to PGV900, I31900, and I44900 exhibited significantly higher nuclear intensities than their respective, as-received counterparts.

The above analysis shows that use of HCI provides a rapid, automated, and unbiased assessment of cell changes as well as a quantitative information on cell counts, cell area, monolayer coverage, and nuclear integrity. The analysis complements previous reports on montmorillonite and fine-sized silica particulate (such as incinerated nanoclay byproduct) which showed both cell damage and cytotoxicity.[54] Mechanisms of silica lung toxicity were shown to include cell membrane penetration, cell lysis, oxygen radical generation, vascular permeability, edema, mitochondrial depolarization, acute and chronic inflammation, apoptosis, pyroptosis, and altered epithelial signaling responses.[54–58]

Except for PGV-exposed cells, loss of monolayer coverage did not align with cell counts, indicating that another mechanism besides cytotoxicity might be driving a decrease in monolayer integrity. As such, an increase in nuclear intensity (i.e., greater DNA material) with no change in nuclear area associated with monolayer integrity loss suggests that surviving bronchial epithelial cells exposed to byproducts had entered a different cell cycle phase compared to unexposed and ONC-exposed cells. Bronchial epithelial cells upon exposure to PM2.5 and other fine particulate, for instance, were shown to display transient G2 arrest, reactive oxygen species (ROS), and inflammation prior to undergoing either apoptosis or wound healing repair acitivity.[59–61]

Our HCI results complement previous studies by Stueckle et al. showing that *in vivo* day 1 postexposure of mouse lung that both Cloisite Na and incinerated Cloisite Na (similar to PGV and PGV900) exhibited acute lung damage and inflammation as revealed in collected bronchoalveolar lavage fluid and histopathological analysis, respectively.[20] Conversely, Cloisite 30B (with a similar coating as I34) displayed a delayed, moderate increase in lung damage at day 7 with minimal damage at day 1 postexposure.

Real-Time Assessment of Cellular Behavior.

BEAS-2B cellular behavior before and after exposure to nanoclays and byproducts was also analyzed as a function of changes in cell-induced impedance signals. ECIS analyses were considered to supplement HCI results since previous reports showed that such screening strategy provides a real-time, high-throughput, noninvasive analysis of quantitative changes in cell morphology and cell–substrate interactions that could be used to monitor behavior, morphology, attachment,[26] and movement of cells.[37,62] ECIS relies on application of an alternating current across an electrode at the bottom of an array to induce a potential evaluated using Ohm's law and has previously shown the ability to monitor cells exposed to a variety of nanomaterials through such real-time, high-throughput, label-free approach.[24,28,63]

Representative ECIS measurements of normalized resistance values of cells exposed to IC_{50} of nanoclays and byproducts were performed for 48 h at 4 kHz frequency and are shown in

Figure 3a (nanoclays) and 3b (byproducts). Currently chosen operational frequency was previously shown to be optimal for measurements of cellular behavior such as cellular membrane integrity, attachment, and cell–cell interactions.[64,65] Our results showed that upon cell seeding the normalized resistance values increased with time due to an increase in sensing area that resulted upon cells settling and interfacing with the electrodes during the 24 h of monolayer formation.[28,62] As the seeded cells developed a confluent monolayer, resistance values tapered off to constant values.[26] After monolayer coverage was recorded, cells were exposed to IC_{50} concentrations of each nanoclay or byproduct in real-time, as described above.

Figure 3a indicates that exposure to nanoclays induced time- and treatment-dependent cellular behavior. Specifically, there was an initial loss of resistance for all exposed cells which was attributed to the electrode being disconnected to ensure cell exposure, followed by an increase in resistance for all cells except those exposed to PGV. Specifically, cells exposed to PGV lost all resistance within 24 h of exposure and exhibited no recovery during the 48 h of observation. Within the period of 2–7 h of exposure, the cells exposed to I31 and I44 showed a slight loss in resistance with respect to controls. From 7 to 24 h, cells exposed to I34 exhibited similar behavior to control cells with a slightly higher resistance, while those exposed to I31 recovered to a resistance value similar to that of the controls. Exposure to I44 also induced a loss in resistance relative to control cells. Furthermore, within the 24–36 h of observation it was noted that cells exposed to I34 showed no changes in overall resistance behavior; however, they held a slightly higher resistance than that of the controls. Complementary, cells exposed to I31 and I44 exhibited a slight rise in resistance relative to controls. From 36 to 48 h of observation no changes in resistance were observed for any of these exposed cells. Final resistance values for cells treated with I31, I34, and I44 were of similar trends to controls, with slightly higher or lower values for I31 and I44, respectively.

Analysis of cellular monolayers exposed to byproducts are shown in Figure 3b and reveal both time- and treatment-dependent response, including major overall differences relative to the nanoclays. Specifically, after an observed initial loss of resistance for all cells (again attributed to the disconnection from the electrode), within the first 2 h of exposure there was an increase in resistance for cells treated with PGV900. From 2 to 10 h, cells exposed to all 4 byproducts showed a loss in resistance relative to controls. While resistances of cells exposed to I31900, I34900, and I44900 were far less than controls, those exhibited by cells exposed to PGV900 were only slightly less than those of the control. During the period of 10–28 h of exposure, no additional changes in resistance were observed. Finally, from 28 to 48 h of observation, cells exposed to all byproducts exhibited steady recovery of resistance however to values far less than those observed for the controls. Relative to one another, I34900 induced the greatest loss in resistance, while I44900 caused the lowest.

Given that one of the cytoskeleton's functions is to regulate cell–substrate interactions[66] and that changes in cellular adhesion may be associated with changes in both cellular morphology[67] and elasticity,[68,69] we also evaluated changes in cell adhesion (i.e., α value) upon exposure to nanoclays or byproducts. Figure 3c and 3d assesses whether there were any restrictions of current pathways beneath the cell monolayers as imposed by such exposures.[26,27] As with the overall resistance measurements, an initial loss in the α value

was noted for all cells (Figure 3c). Within the first hour of exposure, however, there was an increase in α. Also, similar to the resistance measurements, PGV induced an immediate and steady reduction in cell adhesion with no observed recovery over the 48 h of observation, all relative to control. While cells exposed to I31 exhibited no significant change in cell attachment with respect to the controls, exposure to I34 and I44 caused a slight, gradual reduction in adhesion during the last 36 h of evaluation. Correspondingly, during the first hour of exposure, an increase in adhesion was observed for all cells exposed to byproducts (Figure 3d). Also, similar to the overall resistance, exposure to PGV900 induced a more dramatic increase in α when compared to the α value of other byproducts or controls.

Overall treatment with all 4 byproducts induced a similar trend of changes in α as it did for changes in overall resistance, namely, it was noted that values for attachment fell with respect to those of the controls in the 2–10 h observation window, began to stabilize from 10 to 26 h, and recovered slightly during the remaining time of observation (up to 48 h). It should also be noted that cells exposed to PGV900 exhibited higher α during the initial 2–26 h; however, they fell back to levels similar to controls for the rest of the observation time. Exposure to the other byproducts induced losses of α with respect to controls; full recovery of α was not observed for any of the samples. Relative to one another, I34900 induced the greatest loss of α, while I44900 caused the lowest.

Our results complement previous studies that showed silica exposure changes bronchial epithelial cell adhesion, attachment, and cell-to-cell signaling.[57,70] Epithelial cells under enhanced inflammatory signaling were also shown to exhibit increased adhesion abilities, which were partially mediated via inflammatory cytokines and NFκB signaling.[71,72]

Observed changes in both resistance and α show that organically modified nanoclays or byproducts induce a time- and dose-dependent cellular behavior, thus confirming the above HSC studies and possibly hinting at changes in cell cycle,[73] attachment,[74] viability,[75] and morphology during cell death.[37,62] For instance, cells exposed to PGV lost all resistance during exposure, further confirming cell death and loss of monolayer coverage, while exposure to ONCs induced varying degrees of changes in monolayer resistance and recovery, dependent on the type of organic modifier, as also shown in the HCI screening.

Our observations also show that the first 10 h of exposure are the most critical and need to be thoroughly monitored since they yield significant changes for cells exposed to almost all nanoclays and byproducts (with the exception of I34 in the resistance measurements). These changes are presumably due to the differentiation of cellular internalization.[76] Indeed, our physicochemical analyses have shown that organo-modification and thermal degradation significantly changed the degree of hydrophobicity and particle–medium interactions. Such parameters were previously shown to influence internalization (e.g., for a variety of materials from titanium dioxide, to organically modified silica, and carbon nanotubes) with such process to occur in the first few hours of exposure[77–80] and be influenced by material's geometry and size,[78,81] surface functionalization,[82] and degree of hydrophobicity.[23] Numerous studies have also shown that decreased particle size in cell culture medium or *in vivo* exposures, due to differences in particle coating and a medium's protein profile, can result in higher particle number and surface area to drastically increase particle toxicity upon

uptake. Similarly, agglomeration of particles can produce the opposite effects resulting in reduced toxicity.[41,83–85] Here, diminished particle size in DMEM medium for I31 and I34 correlated with increased acute cytotoxicity (i.e., IC_{50} values). The influence on cell behavior was shown to persist with changes in elastic properties or cycle all the way to 12 h of observation.[86] Although cells exposed to I31 and I44 exhibited reduction of resistance initially, we observed their recovery to values similar to those of the controls. This suggests either overall cellular recovery or adaptation to the environment. Indeed, Kim et al. previously found that cells can adapt to nanoparticle uptake and still continue their cell cycle.[87] It should be noted, however, that this recovery of resistance was not observed for cells exposed to the byproducts, further indicating different possible mechanism of toxicity.

Evaluation of Early/Late Apoptosis, Necrosis, and Cell Metabolism.

With the above results and complementing studies by Yoshida et al. showing that organically modifying particles with amine or carboxyl groups reduces the amount of generated reactive oxygen species and DNA damage in HaCaT and TLR-1 cells[88] as well as with Sharma et al. showing that genotoxic effects of nanoclays, such as DNA strand-breaks, in Caco-2 cells were induced by the presence of quaternary ammonium compounds (QAC)s,[89] we were also motivated to identify any programmed cell death mechanisms resulted upon cellular exposure. To ensure high-throughput screening and thus complement both HCI and ECIS, we employed flow cytometry evaluations of cells stained with Annexin V-FITC and PI (Figure 4). Representative flow cytometry scatter plots of control (unexposed) cells and cells exposed to nanoclays or byproducts are shown in Figure 4a; representative flow cytometry scatter plots of particle-only controls to distinguish the effects of particle–dye interactions are shown in Figure S5.

Our analysis (Figure 4b) showed that significantly higher levels of apoptosis and necrosis were induced, relative to control cells, following short-term exposure (for 24 h) to IC_{50} concentrations of both nanoclays and byproducts. Specifically, exposure to both PGV and I31 induced significantly higher percentages of cells in early apoptosis (23% and 13%, respectively) relative to control cells (3%). However, exposure to I34 and I44 did not significantly change the percentages of cells in early apoptosis (6.56% and 6.08%, respectively). Additionally, we observed significantly higher percentages of cells in late apoptosis upon exposure to I31 and I44 (12% each) relative to control cells (3.6%). However, neither PGV nor I34 induced significantly higher percentages of late apoptotic cells (2.98% and 4.93%, respectively). Lastly, levels of necrotic cells were significantly higher than controls (1.2%) following exposure to I31 and I44 (2.4% and 3.4%, respectively) but not upon exposure to PGV and I34 (0.48% and 1.45%, respectively).

Complementary, exposure to byproducts did not induce a significant increase in either early or late apoptotic cells with respect to controls. However, exposure to all 4 byproducts caused significantly higher percentages of necrotic cells (4% for PGV900, 3.4% for I31900, 3.3% for I34900, and 3.4% for I44900) with respect to controls (1.2%). Levels of early apoptotic cells upon exposure to PGV900 (4.7%) and I31900 (3.1%) were significantly different from those induced by PGV and I31, respectively. Furthermore, levels of late apoptotic cells upon exposure to I31900 (4.7%) and I44900 (5.1%) were significantly different from those

induced by I31 and I44, respectively. Finally, levels of necrotic cells were significantly different for PGV900, I31900, and I34900 with respect to their as-received counterparts.

Our results further confirm that the presence and type of organic modifier induces different levels of cell death. For instance, I31 induced a much wider range of cell death, while I44 was shown to only induce significantly higher levels of late apoptosis and necrosis, both relative to controls.

These differences again support the hypothesis that the mechanism of toxicity depends on the differences in organo-modification of the nanoclays.[90] Specifically, the modifier for I31 (Figure S1) contains a silane coupling agent used to interact with polymers to a dissimilar material such as silica or alumina oxide.[91] This compound may also cause interaction with biomolecules with inherent hydroxyl groups[92] or the cell membrane[93] resulting in upper respiratory tract toxicities.[94] In addition, positively charged octadecylamine (i.e., stearylamine) would interact with negatively charged phospholipid membranes, increasing lung inflammatory response, cell necrosis, and apoptosis.[95–99]

Complementary, both of the organic modifiers in I31 and I44 contained alkyl chains with a polar cationic headgroup. Cationic lipids are known to possess unique abilities to interact with plasma membranes and are heavily studied in liposome nonviral delivery research; however, they have exhibited cytotoxic effects including induction of cell necrosis, destabilization of endosomes following endocytosis, ROS production, and ultimately apoptosis.[100,101] Furthermore, the hydroxyl groups located within the organic modifier of I34 has significant potential for bioreactivity. It has been shown, for instance, that such group can interact with cellular molecules, cause membrane damage, and induce apoptosis.[14,102,103] Exposure to another nanoclay (Cloisite 30B) with similar organic modifier to I34 was found, for instance, to induce changes in lipid metabolism, altered Golgi apparatus, and increased mitochondrial degeneration,[104] which could lead to ROS and potential apoptotic cell death. These mechanisms of cell toxicity drastically differ from those well documented for uncoated crystalline silica (i.e., PGV), which are known to include silanol-induced plasma membrane disruption, lysis, mitochondrial depolarization, and apoptosis.[54]

These high-throughput results are supported by the changes in cellular viability before and after exposure to IC_{50} concentrations of nanoclays or byproducts as supplemented by water-soluble tetrazolium salt (WST-1) assay. Briefly, exposure to PGV led to a significant loss of cellular viability (1%) with respect to controls (unexposed cells) with slight recovery after 48 and 72 h of observation time (10% and 13%, respectively; Figure 5a). Furthermore, cells exposed to I31, I34, and I44 exhibited significantly reduced viability (52%, 51%, and 42%, respectively) after 24 h of exposure, all relative to controls. After 48 and 72 h of exposure, however, full viability recovery (when compared to controls) for cells exposed to both I31 and I34 (107% and 93%, respectively) was observed. Although cells exposed to I44 recovered viability (87%) after 48 h of exposure, a second loss of cellular viability was observed after 72 h (with samples exhibiting 23% of the control values), thus possibly indicating a delayed toxic response.

Additionally, exposure to IC_{50} concentrations of byproducts induced changes in cellular viability (Figure 5b). Cells exposed to all four thermally degraded byproducts exhibited significant loss of cellular viability at 24 (PGV900 at 36%, I31900 at 18%, I34900 at 37%, and I44900 at 30%), 48 (46%, 46%, 46%, and 45%, respectively), and 72 h (38%, 29%, 34%, and 23%, respectively) relative to control cells. Only slight recovery of viability was observed for cells exposed to byproducts when compared to controls after 48 and 72 h. Furthermore, at all 3 time points viability for the cells exposed to PGV900 was significantly higher than that for those exposed to PGV. Additionally, cellular viability upon exposure to I31900 and I34900 was significantly different than that of their respective counterparts after 48 and 72 h. Treatment with I44900, for instance, induced significantly different cellular viability with respect to treatment with I44 at only the 48 h time point.

Proposed Mechanisms Responsible for Differences in Cell Behavior.

In comparing our novel findings with available nanoclay toxicity literature, several interesting observations are notable and could represent avenues of further research efforts. Specifically, the difference in mechanism of cell death observed for the different ONC exposures may be attributed to the potential of these positively charged organic modifier chains to influence changes in structure of the lipid membrane as well as to provoke changes in cell signaling.[105] This is supported by previous research that showed that surface functionalization of nanoparticles with fatty acids influence the rate of cellular uptake, presumably due to the interactions with the lipid membrane.[106]

Additionally, we noted that mechanisms of cell death for byproducts were similar to one another but dissimilar from their as-received counterparts. This is again presumably due to loss of the organic modifiers (and their respective induced bioactivities), silanol groups, and platelet structure. Specifically, Verma et al. found that platelet-type nanoclays induced greater toxicity on the lung epithelial cell line A549 than tubular-type nanoclays.[107] Complementary, Zhang et al. found that pyrolytic amorphous silica (comparable to PGV900) induced an ROS-dependent pathway of toxicity in erythrocytes with eventual hemolysis.[108] Furthermore, Zhang et al. showed that toxicity of amorphous silica was dependent on the framework and its surface chemistry, triggering differences in inflammation response[108] with studies by Schreider et al. and Stueckle et al. both reporting that incinerated montmorillonite causes pulmonary inflammation and potentially increases risk for fibrosis development.[20,55]

Previous investigations into nanoclay-induced toxicity have shown that exposure to these particles could activate different cellular responses such as oxidative stress,[77,109] membrane damage,[110] mitochondrial dysfunction,[110] micronucleation,[111] and DNA damage[89,112] and be responsible for cell apoptosis.[77] Furthermore, these toxic effects were shown to change given differences in aspect ratio, organo-modification, and agglomeration of the nanoclays. Our observation of significant loss of cellular viability upon exposure to pristine nanoclay mirrors well the knowledge that surface groups such as silanol and aluminum oxide cause inflammation and membrane damage.[54,113] Additionally, Kondej et al. and Mousseau et al. have recently shown that bentonite and nanoalumina, respectively, both interact with lung

surfactant, which may induce a change in the manner of particle interaction with lung cells.[114,115]

Moreover, we show that cells exposed to I31, I34, and I44 lost 50% viability (with respect to controls) after 24 h of exposure, confirming IC_{50} values.[23] These results further suggest a difference in mechanism of action of these ONCs when compared to pristine nanoclay, possibly indicating significant loss of NADH metabolism (as confirmed by WST-1 assay), but no loss of monolayer coverage (as confirmed by both HCI and ECIS). Sublethal concentrations of soluble QACs were previously shown to cause mitochondrial fragmentation, inhibition of complex I, and slowed ADP phosphorylation to result in reduced cellular energy charge in columnar epithelial cells.[116] This reduction in cellular energy can induce apoptosis, while higher doses induce necrosis or cell lysis.[117] Furthermore, within 48 h of exposure, cells exposed to the tested samples showed viabilities similar to control cells, indicating likely recovery. Note that cells exposed to I44 again lost viability after 72 h of exposure, indicating a delayed toxic response. This is presumably due to dissolution of the modifier over time. These observations indicate that both the presence and the type of organic modifier as well as incineration status drive toxicity *in vitro*.

CONCLUSIONS

Our work aimed to provide an assessment of toxicity for a library of nanoclays and their byproducts to help represent the life cycle of these materials. Using high-content imaging and real-time, cell-based cytotoxicity assays we showed that exposure of human lung epithelial cells to these nanoclays or byproducts lead to changes in monolayer integrity, cellular behavior, and adhesion to all influence the mechanism of cell death in a manner dependent on the physicochemical properties of the individual sample. Specifically, the type and presence of organo-modification and incineration status significantly changed the surface chemistry and size distribution of the nanoclays and byproducts, which elicited differential cellular responses. Pristine nanoclay caused acute loss of monolayer integrity, increased cytotoxicity and apoptosis, while ONCs retained monolayer integrity coupled with inducing differential apoptosis and cell metabolism responses. Incinerated nanoclays caused cell monolayer damage, necrosis, and little evidence of monolayer recovery. Future work must focus on elucidating the mechanism of pulmonary toxicity for these nanoparticles using complementary *in vitro* and *in vivo* models. Combining such *in vitro* approaches with *in silico* and 3D models could improve alternative testing strategies and help identify key events in adverse outcome pathways to establish the predictability of human responses upon exposures to materials with different physicochemical characteristics. A better understanding of the effects of such properties on toxicity, including on the immune, airway, and alveolar epithelial cell perturbations, could lead to improved prevention by material-based design strategies for enhanced safety practices.

Supplementary Material

Refer to Web version on PubMed Central for supplementary material.

Acknowledgments

Funding

Support for this work was through the National Institutes of Health (R01-ES022968), NIOSH Nanotechnology Research Center 921043S, and IGERT program at West Virginia University (WVU). The authors acknowledge use of WVU Shared Research Facilities and the WVU Flow Cytometry Core Facility (supported by the NIH equipment grant number S10OD016165 and the Institutional Development Award (IDeA) from the National Institute of General Medical Sciences of the NIH under grant numbers P30GM103488 (CoBRE) and P20GM103434 (INBRE)).

The findings and conclusions in this article are those of the authors and do not necessarily represent the view of the National Institute for Occupational Safety and Health, Centers for Disease Control and Prevention.

REFERENCES

(1). The Global Market for Graphene; Future Markets, 2017; pp 204–212.

(2). McWilliams A. Nanocomposites, Nanoparticles, Nanoclays, and Nanotubes; BCC Publishing, 2010; p 144.

(3). The global market for nanoclays, 2010–2025; Future Markets, 2015; p 41.

(4). Yang Y, and Westerhoff P. (2014) Presence in, and release of, nanomaterials from consumer products. Adv. Exp. Med. Biol. 811, 1–17. [PubMed: 24683024]

(5). Mackevica A, and Foss Hansen S. (2016) Release of nanomaterials from solid nanocomposites and consumer exposure assessment - a forward-looking review. Nanotoxicology 10 (6), 641–53. [PubMed: 26667577]

(6). Debia M, Bakhiyi B, Ostiguy C, Verbeek JH, Brouwer DH, and Murashov V. (2016) A Systematic Review of Reported Exposure to Engineered Nanomaterials. Ann. Occup. Hyg. 60 (8), 916–35. [PubMed: 27422281]

(7). Roes L, Patel MK, Worrell E, and Ludwig C. (2012) Preliminary evaluation of risks related to waste incineration of polymer nanocomposites. Sci. Total Environ. 417–418, 76–86.

(8). Nowack B, Ranville JF, Diamond S, Gallego-Urrea JA, Metcalfe C, Rose J, Horne N, Koelmans AA, and Klaine SJ (2012) Potential scenarios for nanomaterial release and subsequent alteration in the environment. Environ. Toxicol. Chem. 31 (1), 50–9. [PubMed: 22038832]

(9). Mitrano DM, Motellier S, Clavaguera S, and Nowack B. (2015) Review of nanomaterial aging and transformations through the life cycle of nano-enhanced products. Environ. Int. 77, 132–47. [PubMed: 25705000]

(10). Zeng SLYZY, Zhang QF, Du YJ, Sun YT, and Zhang MJ (1998) Study on occupational standard of bentonite dust in air of workplace. Chin. J. Ind. Hyg. Occup. Dis. 16, 177–178.

(11). Huang Y, Zhang M, Zou H, Li X, Xing M, Fang X, and He J. (2013) Genetic damage and lipid peroxidation in workers occupationally exposed to organic bentonite particles. Mutat. Res., Genet. Toxicol. Environ. Mutagen. 751 (1), 40–44.

(12). Holder AL, Vejerano EP, Zhou X, and Marr LC (2013) Nanomaterial disposal by incineration. Environ. Sci. Process Impacts 15 (9), 1652–64. [PubMed: 23880913]

(13). Part F, Zecha G, Causon T, Sinner EK, and Huber-Humer M. (2015) Current limitations and challenges in nanowaste detection, characterisation and monitoring. Waste Manage. 43, 407–20.

(14). Sotiriou GA, Singh D, Zhang F, Chalbot MG, Spielman-Sun E, Hoering L, Kavouras IG, Lowry GV, Wohlleben W, and Demokritou P. (2016) Thermal decomposition of nano-enabled thermoplastics: Possible environmental health and safety implications. J. Hazard. Mater. 305, 87–95. [PubMed: 26642449]

(15). Buha J, Mueller N, Nowack B, Ulrich A, Losert S, and Wang J. (2014) Physical and chemical characterization of fly ashes from Swiss waste incineration plants and determination of the ash fraction in the nanometer range. Environ. Sci. Technol. 48 (9), 4765–73. [PubMed: 24720846]

(16). Wagner A, White AP, Tang MC, Agarwal S, Stueckle TA, Rojanasakul Y, Gupta RK, and Dinu CZ (2018) Incineration of Nanoclay Composites Leads to Byproducts with Reduced Cellular Reactivity. Sci. Rep. 8 (1), 10709. [PubMed: 30013129]

(17). Pourchez J, Chivas-Joly C, Longuet C, Leclerc L, Sarry G, and Lopez-Cuesta JM (2018) End-of-life incineration of nanocomposites: new insights into nanofiller partitioning into by-products and biological outcomes of airborne emission and residual ash. Environ. Sci.: Nano 5 (8), 1951–1964.

(18). Chivas-Joly C, Longuet C, Pourchez J, Leclerc L, Sarry G, and Lopez-Cuesta JM (2019) Physical, morphological and chemical modification of Al-based nanofillers in by-products of incinerated nanocomposites and related biological outcome. J. Hazard. Mater. 365, 405–412. [PubMed: 30448553]

(19). Bentonite, kaolin and selected clay minerals; World Health Organization, 2015; Vol. 231, p 159.

(20). Stueckle TA, Davidson DC, Derk R, Kornberg TG, Battelli L, Friend S, Orandle M, Wagner A, Dinu CZ, Sierros KA, Agarwal S, Gupta RK, Rojanasakul Y, Porter DW, and Rojanasakul L. (2018) Short-Term Pulmonary Toxicity Assessment of Pre- and Post-incinerated Organomodified Nanoclay in Mice. ACS Nano 12 (3), 2292–2310. [PubMed: 29451776]

(21). Nonfatal occupational injuries and illnesses requiring days away from work: 2013; U.S. Bureau of Labor Statistics, 2014.

(22). Chronic obstructive pulmonary disease: estimated prevalence by current industry, US working adults aged 18 and over, 2004–2011; Centers for Disease Control and Prevention, 2014.

(23). Wagner A, White AP, Stueckle TA, Banerjee D, Sierros KA, Rojanasakul Y, Agarwal S, Gupta RK, and Dinu CZ (2017) Early Assessment and Correlations of Nanoclay's Toxicity to Their Physical and Chemical Properties. ACS Appl. Mater. Interfaces 9 (37), 32323–32335. [PubMed: 28799741]

(24). Wagner A, Eldawud R, White A, Agarwal S, Stueckle TA, Sierros KA, Rojanasakul Y, Gupta RK, and Dinu CZ (2017) Toxicity evaluations of nanoclays and thermally degraded byproducts through spectroscopical and microscopical approaches. Biochim. Biophys. Acta, Gen. Subj. 1861 (1), 3406–3415. [PubMed: 27612663]

(25). Xiao C, Lachance B, Sunahara G, and Luong JH (2002) Assessment of cytotoxicity using electric cell-substrate impedance sensing: concentration and time response function approach. Anal. Chem. 74 (22), 5748–53. [PubMed: 12463358]

(26). Xiao C, Lachance B, Sunahara G, and Luong JH (2002) An in-depth analysis of electric cell-substrate impedance sensing to study the attachment and spreading of mammalian cells. Anal. Chem. 74 (6), 1333–9. [PubMed: 11924593]

(27). Eldawud R, Stueckle TA, Manivannan S, Elbaz H, Chen M, Rojanasakul Y, and Dinu CZ (2014) Real-time analysis of the effects of toxic, therapeutic and sub-therapeutic concentrations of digitoxin on lung cancer cells. Biosens. Bioelectron. 59, 192–9. [PubMed: 24727605]

(28). Eldawud R, Wagner A, Dong C, Rojansakul Y, and Zoica Dinu C. (2015) Electronic platform for real-time multi-parametric analysis of cellular behavior post-exposure to single-walled carbon nanotubes. Biosens. Bioelectron. 71, 269–277. [PubMed: 25913448]

(29). Slater TF, Sawyer B, and Straeuli U. (1963) Studies on Succinate-Tetrazolium Reductase Systems. Iii. Points of Coupling of Four Different Tetrazolium Salts. Biochim. Biophys. Acta 77, 383–93. [PubMed: 14089413]

(30). Yin LM, Wei Y, Wang Y, Xu YD, and Yang YQ (2013) Long term and standard incubations of WST-1 reagent reflect the same inhibitory trend of cell viability in rat airway smooth muscle cells. Int. J. Med. Sci. 10 (1), 68–72. [PubMed: 23289007]

(31). Geraci C, Heidel D, Sayes C, Hodson L, Schulte P, Eastlake A, and Brenner S. (2015) Perspectives on the design of safer nanomaterials and manufacturing processes. J. Nanopart. Res. 17 (9), 366. [PubMed: 26435688]

(32). Härkki O Biaxially oriented PLA-montmorillonite-nanocomposite for barrier film applications Research highlights in industrial biomaterials; VTT: Espoo, 2012; Vol. 2, pp 59–62.

(33). Feng J, Hao J, Du J, and Yang R. (2012) Effects of organoclay modifiers on the flammability, thermal and mechanical properties of polycarbonate nanocomposites filled with a phosphate and organoclays. Polym. Degrad. Stab. 97 (1), 108–117.

(34). Yourdkhani M, Mousavand T, Chapleau N, and Hubert P. (2013) Thermal, oxygen barrier and mechanical properties of polylactide-organoclay nanocomposites. Compos. Sci. Technol. 82, 47–53.

(35). Campos-Requena VH, Rivas BL, Pérez MA, Garrido-Miranda KA, and Pereira ED (2015) Polymer/clay nanocomposite films as active packaging material: Modeling of antimicrobial release. Eur. Polym. J. 71, 461–475.

(36). Tang Y, and Lewin M. (2007) Maleated polypropylene OMMT nanocomposite: Annealing, structural changes, exfoliated and migration. Polym. Degrad. Stab. 92 (1), 53–60.

(37). Wegener J, Keese CR, and Giaever I. (2000) Electric cell-substrate impedance sensing (ECIS) as a noninvasive means to monitor the kinetics of cell spreading to artificial surfaces. Exp. Cell Res. 259 (1), 158–66. [PubMed: 10942588]

(38). Lo CM, Keese CR, and Giaever I. (1995) Impedance analysis of MDCK cells measured by electric cell-substrate impedance sensing. Biophys. J. 69 (6), 2800–7. [PubMed: 8599686]

(39). Warheit DB, Webb TR, Sayes CM, Colvin VL, and Reed KL (2006) Pulmonary instillation studies with nanoscale TiO2 rods and dots in rats: toxicity is not dependent upon particle size and surface area. Toxicol. Sci. 91 (1), 227–36. [PubMed: 16495353]

(40). Nel A, Xia T, Madler L, and Li N. (2006) Toxic potential of materials at the nanolevel. Science 311 (5761), 622–7. [PubMed: 16456071]

(41). Lordan S, and Higginbotham CL (2012) Effect of serum concentration on the cytotoxicity of clay particles. Cell Biol. Int. 36 (1), 57–61. [PubMed: 21883092]

(42). Shannahan JH, Brown JM, Chen R, Ke PC, Lai X, Mitra S, and Witzmann FA (2013) Comparison of nanotube-protein corona composition in cell culture media. Small 9 (12), 2171–81. [PubMed: 23322550]

(43). Zeinabad HA, Zarrabian A, Saboury AA, Alizadeh AM, and Falahati M. (2016) Interaction of single and multi wall carbon nanotubes with the biological systems: tau protein and PC12 cells as targets. Sci. Rep. 6, 26508. [PubMed: 27216374]

(44). Moore TL, Rodriguez-Lorenzo L, Hirsch V, Balog S, Urban D, Jud C, Rothen-Rutishauser B, Lattuada M, and PetriFink A. (2015) Nanoparticle colloidal stability in cell culture media and impact on cellular interactions. Chem. Soc. Rev. 44 (17), 6287–305. [PubMed: 26056687]

(45). Braga VM, Del Maschio A, Machesky L, and Dejana E. (1999) Regulation of cadherin function by Rho and Rac: modulation by junction maturation and cellular context. Mol. Biol. Cell 10 (1), 9–22. [PubMed: 9880323]

(46). Levesque JP, and Simmons PJ (1999) Cytoskeleton and integrin-mediated adhesion signaling in human CD34+ hemopoietic progenitor cells. Exp. Hematol. 27 (4), 579–86. [PubMed: 10210315]

(47). Knights AJ, Funnell AP, Crossley M, and Pearson RC (2012) Holding Tight: Cell Junctions and Cancer Spread. Trends Cancer Res. 8, 61–69. [PubMed: 23450077]

(48). Savagner P Rise and Fall of Epithelial Phenotype: Concepts of Epithelial-Mesenchymal Transition; Kluwer Academic/Plenum, 2007; Vol. 248, p 101.

(49). Park YH, Kim D, Dai J, and Zhang Z. (2015) Human bronchial epithelial BEAS-2B cells, an appropriate in vitro model to study heavy metals induced carcinogenesis. Toxicol. Appl. Pharmacol. 287 (3), 240–5. [PubMed: 26091798]

(50). Siegrist KJ, Reynolds SH, Kashon ML, Lowry DT, Dong C, Hubbs AF, Young SH, Salisbury JL, Porter DW, Benkovic SA, McCawley M, Keane MJ, Mastovich JT, Bunker KL, Cena LG, Sparrow MC, Sturgeon JL, Dinu CZ, and Sargent LM (2014) Genotoxicity of multi-walled carbon nanotubes at occupationally relevant doses. Part. Fibre Toxicol. 11, 6. [PubMed: 24479647]

(51). Gangwal S, Brown JS, Wang A, Houck KA, Dix DJ, Kavlock RJ, and Hubal EA (2011) Informing selection of nanomaterial concentrations for ToxCast in vitro testing based on occupational exposure potential. Environ. Health Perspect. 119 (11), 1539–46. [PubMed: 21788197]

(52). Hubbs A, Greskevitch M, Kuempel E, Suarez F, and Toraason M. (2005) Abrasive blasting agents: designing studies to evaluate relative risk. J. Toxicol. Environ. Health, Part A 68 (11–12), 999–1016.

(53). Kalluri R. (2009) EMT: when epithelial cells decide to become mesenchymal-like cells. J. Clin. Invest. 119 (6), 1417–9. [PubMed: 19487817]

(54). Pavan C, and Fubini B. (2017) Unveiling the Variability of ″Quartz Hazard″ in Light of Recent Toxicological Findings. Chem. Res. Toxicol. 30 (1), 469–485. [PubMed: 27992190]

(55). Schreider JP, Culbertson MR, and Raabe OG (1985) Comparative pulmonary fibrogenic potential of selected particles. Environ. Res. 38 (2), 256–74. [PubMed: 4065076]

(56). Fruijtier-Polloth C. (2012) The toxicological mode of action and the safety of synthetic amorphous silica-a nanostructured material. Toxicology 294 (2–3), 61–79. [PubMed: 22349641]

(57). Perkins TN, Peeters PM, Shukla A, Arijs I, Dragon J, Wouters EF, Reynaert NL, and Mossman BT (2015) Indications for distinct pathogenic mechanisms of asbestos and silica through gene expression profiling of the response of lung epithelial cells. Hum. Mol. Genet. 24 (5), 1374–89. [PubMed: 25351596]

(58). Perkins TN, Dentener MA, Stassen FR, Rohde GG, Mossman BT, Wouters EF, and Reynaert NL (2016) Alteration of canonical and non-canonical WNT-signaling by crystalline silica in human lung epithelial cells. Toxicol. Appl. Pharmacol. 301, 61–70. [PubMed: 27095093]

(59). Longhin E, Holme JA, Gutzkow KB, Arlt VM, Kucab JE, Camatini M, and Gualtieri M. (2013) Cell cycle alterations induced by urban PM2.5 in bronchial epithelial cells: characterization of the process and possible mechanisms involved. Part. Fibre Toxicol. 10, 63. [PubMed: 24354623]

(60). Wu J, Shi Y, Asweto CO, Feng L, Yang X, Zhang Y, Hu H, Duan J, and Sun Z. (2017) Fine particle matters induce DNA damage and G2/M cell cycle arrest in human bronchial epithelial BEAS-2B cells. Environ. Sci. Pollut. Res. 24 (32), 25071–25081.

(61). Loxham M, Morgan-Walsh RJ, Cooper MJ, Blume C, Swindle EJ, Dennison PW, Howarth PH, Cassee FR, Teagle DA, Palmer MR, and Davies DE (2015) The effects on bronchial epithelial mucociliary cultures of coarse, fine, and ultrafine particulate matter from an underground railway station. Toxicol. Sci. 145 (1), 98–107. [PubMed: 25673499]

(62). Giaever I, and Keese CR (1991) Micromotion of mammalian cells measured electrically. Proc. Natl. Acad. Sci. U. S. A. 88 (17), 7896–900. [PubMed: 1881923]

(63). Eldawud R, Reitzig M, Opitz J, Rojansakul Y, Jiang W, Nangia S, and Dinu CZ (2016) Combinatorial approaches to evaluate nanodiamond uptake and induced cellular fate. Nanotechnology 27 (8), 085107.

(64). Re F, Zanetti A, Sironi M, Polentarutti N, Lanfrancone L, Dejana E, and Colotta F. (1994) Inhibition of anchorage-dependent cell spreading triggers apoptosis in cultured human endothelial cells. J. Cell Biol. 127 (2), 537–46. [PubMed: 7523422]

(65). Hussain S, Thomassen LC, Ferecatu I, Borot MC, Andreau K, Martens JA, Fleury J, Baeza-Squiban A, Marano F, and Boland S. (2010) Carbon black and titanium dioxide nanoparticles elicit distinct apoptotic pathways in bronchial epithelial cells. Part. Fibre Toxicol. 7, 10. [PubMed: 20398356]

(66). Yamada KM, and Geiger B. (1997) Molecular interactions in cell adhesion complexes. Curr. Opin. Cell Biol. 9 (1), 76–85. [PubMed: 9013677]

(67). Song M, Zeng L, Yuan S, Yin J, Wang H, and Jiang G. (2013) Study of cytotoxic effects of single-walled carbon nanotubes functionalized with different chemical groups on human MCF7 cells. Chemosphere 92 (5), 576–82. [PubMed: 23648328]

(68). Dong C, Campell AS, Eldawud R, Perhinschi G, Rojanasakul Y, and Dinu CZ (2013) Effects of acid treatment on structure, properties and biocompatibility of carbon nanotubes. Appl. Surf. Sci. 264, 261–268.

(69). Dong C, Eldawud R, Sargent LM, Kashon ML, Lowry D, Rojanasakul Y, and Dinu CZ (2014) Towards Elucidating the Effects of Purified MWCNTs on Human Lung Epithelial cells. Environ. Sci.: Nano 1 (6), 595–603.

(70). Kasper J, Hermanns MI, Bantz C, Maskos M, Stauber R, Pohl C, Unger RE, and Kirkpatrick JC (2011) Inflammatory and cytotoxic responses of an alveolar-capillary coculture model to silica nanoparticles: comparison with conventional monocultures. Part. Fibre Toxicol. 8 (1), 6. [PubMed: 21272353]

(71). Leir SH, Holgate ST, and Lackie PM (2003) Inflammatory cytokines can enhance CD44-mediated airway epithelial cell adhesion independently of CD44 expression. Am. J. Physiol Lung Cell Mol. Physiol 285 (6), L1305–11. [PubMed: 12909589]

(72). Ward C, Schlingmann B, Stecenko AA, Guidot DM, and Koval M. (2015) NF-kappaB inhibitors impair lung epithelial tight junctions in the absence of inflammation. Tissue Barriers 3 (1–2), e982424. [PubMed: 25838984]

(73). Wang L, Wang L, Yin H, Xing W, Yu Z, Guo M, and Cheng J. (2010) Real-time, label-free monitoring of the cell cycle with a cellular impedance sensing chip. Biosens. Bioelectron. 25 (5), 990–5. [PubMed: 19818595]

(74). Xiao C, and Luong JH (2005) Assessment of cytotoxicity by emerging impedance spectroscopy. Toxicol. Appl. Pharmacol. 206 (2), 102–12. [PubMed: 15967198]

(75). Male KB, Lachance B, Hrapovic S, Sunahara G, and Luong JH (2008) Assessment of cytotoxicity of quantum dots and gold nanoparticles using cell-based impedance spectroscopy. Anal. Chem. 80 (14), 5487–93. [PubMed: 18553941]

(76). Storm G, Belliot SO, Daemen T, and Lasic DD (1995) Surface modification of nanoparticles to oppose uptake by the mononuclear phagocyte system. Adv. Drug Delivery Rev. 17 (1), 31–48.

(77). Baek M, Kim IS, Yu J, Chung HE, Choy JH, and Choi SJ (2011) Effect of different forms of anionic nanoclays on cytotoxicity. J. Nanosci. Nanotechnol. 11 (2), 1803–6. [PubMed: 21456296]

(78). Lu F, Wu SH, Hung Y, and Mou CY (2009) Size effect on cell uptake in well-suspended, uniform mesoporous silica nanoparticles. Small 5 (12), 1408–13. [PubMed: 19296554]

(79). Roy I, Ohulchanskyy TY, Bharali DJ, Pudavar HE, Mistretta RA, Kaur N, and Prasad PN (2005) Optical tracking of organically modified silica nanoparticles as DNA carriers: a nonviral, nanomedicine approach for gene delivery. Proc. Natl. Acad. Sci. U. S. A. 102 (2), 279–84. [PubMed: 15630089]

(80). Stearns RC, Paulauskis JD, and Godleski JJ (2001) Endocytosis of ultrafine particles by A549 cells. Am. J. Respir. Cell Mol. Biol. 24 (2), 108–15. [PubMed: 11159043]

(81). Herd H, Daum N, Jones AT, Huwer H, Ghandehari H, and Lehr CM (2013) Nanoparticle geometry and surface orientation influence mode of cellular uptake. ACS Nano 7 (3), 1961–73. [PubMed: 23402533]

(82). Slowing I, Trewyn BG, and Lin VS (2006) Effect of surface functionalization of MCM-41-type mesoporous silica nanoparticles on the endocytosis by human cancer cells. J. Am. Chem. Soc. 128 (46), 14792–3. [PubMed: 17105274]

(83). Konduru NV, Molina RM, Swami A, Damiani F, Pyrgiotakis G, Lin P, Andreozzi P, Donaghey TC, Demokritou P, Krol S, Kreyling W, and Brain JD (2017) Protein corona: implications for nanoparticle interactions with pulmonary cells. Part. Fibre Toxicol. 14 (1), 42. [PubMed: 29084556]

(84). Cohen JM, Teeguarden JG, and Demokritou P. (2014) An integrated approach for the in vitro dosimetry of engineered nanomaterials. Part. Fibre Toxicol. 11, 20. [PubMed: 24885440]

(85). Pal AK, Bello D, Cohen J, and Demokritou P. (2015) Implications of in vitro dosimetry on toxicological ranking of low aspect ratio engineered nanomaterials. Nanotoxicology 9 (7), 871–85. [PubMed: 25672815]

(86). Dong C, Kashon ML, Lowry D, Dordick JS, Reynolds SH, Rojanasakul Y, Sargent LM, and Dinu CZ (2013) Exposure to carbon nanotubes leads to changes in the cellular biomechanics. Adv. Healthcare Mater. 2 (7), 945–51.

(87). Kim JA, Aberg C, Salvati A, and Dawson KA (2012) Role of cell cycle on the cellular uptake and dilution of nanoparticles in a cell population. Nat. Nanotechnol. 7 (1), 62–8.

(88). Yoshida T, Yoshioka Y, Matsuyama K, Nakazato Y, Tochigi S, Hirai T, Kondoh S, Nagano K, Abe Y, Kamada H, Tsunoda S, Nabeshi H, Yoshikawa T, and Tsutsumi Y. (2012) Surface modification of amorphous nanosilica particles suppresses nanosilica-induced cytotoxicity, ROS generation, and DNA damage in various mammalian cells. Biochem. Biophys. Res. Commun. 427 (4), 748–52. [PubMed: 23044420]

(89). Sharma AK, Schmidt B, Frandsen H, Jacobsen NR, Larsen EH, and Binderup ML (2010) Genotoxicity of unmodified and organo-modified montmorillonite. Mutat. Res., Genet. Toxicol. Environ. Mutagen. 700 (1–2), 18–25.

(90). Janer G, Fernandez-Rosas E, Mas del Molino E, Gonzalez-Galvez D, Vilar G, Lopez-Iglesias C, Ermini V, and Vazquez-Campos S. (2014) In vitro toxicity of functionalised nanoclays is mainly driven by the presence of organic modifiers. Nanotoxicology 8 (3), 279–94. [PubMed: 23405880]

(91). Sterman S, and Marsden JG (1966) Silane coupling agents. Ind. Eng. Chem. 58 (3), 33–37.

(92). Soteropulos CE, and Hunt HK (2012) Attaching biological probes to silica optical biosensors using silane coupling agents. J. Visualized Exp. No. 63, 3866.

(93). Ojea-Jiménez I, Urbán P, Barahona F, Pedroni M, Capomaccio R, Ceccone G, Kinsner-Ovaskainen A, Rossi F, and Gilliland D. (2016) Highly Flexible Platform for Tuning Surface Properties of Silica Nanoparticles and Monitoring Their Biological Interaction. ACS Appl. Mater. Interfaces 8 (7), 4838–4850. [PubMed: 26779668]

(94). OECD Screening Information Data Set for 3-Aminopropyltriethoxysilane [APTES]; International Programme on Chemical Safety, 2003; p 123.

(95). Andersen FA (1995) Final report on the safety assessment of lauramine and stearamine. J. Am. Coll. Toxicol. 14 (3), 196–203.

(96). Harush-Frenkel O, Bivas-Benita M, Nassar T, Springer C, Sherman Y, Avital A, Altschuler Y, Borlak J, and Benita S. (2010) A safety and tolerability study of differently-charged nanoparticles for local pulmonary drug delivery. Toxicol. Appl. Pharmacol. 246 (1–2), 83–90. [PubMed: 20417650]

(97). Fischer D, Li Y, Ahlemeyer B, Krieglstein J, and Kissel T. (2003) In vitro cytotoxicity testing of polycations: influence of polymer structure on cell viability and hemolysis. Biomaterials 24 (7), 1121–31. [PubMed: 12527253]

(98). Jonas AJ, and Speller RJ (1989) Stearylamine permeabilizes the lysosomal membrane to cystine and sialic acid. Biochim. Biophys. Acta, Biomembr. 984 (3), 257–61.

(99). De M, Ghosh S, Sen T, Shadab M, Banerjee I, Basu S, and Ali N. (2018) A Novel Therapeutic Strategy for Cancer Using Phosphatidylserine Targeting Stearylamine-Bearing Cationic Liposomes. Mol. Ther.–Nucleic Acids 10, 9–27. [PubMed: 29499959]

(100). Simberg D, Weisman S, Talmon Y, and Barenholz Y. (2004) DOTAP (and other cationic lipids): chemistry, biophysics, and transfection. Crit. Rev. Ther. Drug Carrier Syst. 21 (4), 257–317. [PubMed: 15638468]

(101). Dokka S, Toledo D, Shi X, Castranova V, and Rojanasakul Y. J. P. r. (2000) Pharm. Res. 17 (5), 521–525. [PubMed: 10888302]

(102). Tarn D, Ashley CE, Xue M, Carnes EC, Zink JI, and Brinker CJ (2013) Mesoporous silica nanoparticle nanocarriers: biofunctionality and biocompatibility. Acc. Chem. Res. 46 (3), 792–801. [PubMed: 23387478]

(103). Das S, Singh S, Singh V, Joung D, Dowding JM, Reid D, Anderson J, Zhai L, Khondaker SI, Self WT, and Seal S. (2013) Oxygenated functional group density on graphene oxide: Its effect on cell toxicity. Particle and Particle Systems Characterization 30 (2), 148–157.

(104). Maisanaba S, Puerto M, Pichardo S, Jorda M, Moreno FJ, Aucejo S, and Jos A. (2013) In vitro toxicological assessment of clays for their use in food packaging applications. Food Chem. Toxicol. 57, 266–75. [PubMed: 23579166]

(105). Ibarguren M, Lopez DJ, and Escriba PV (2014) The effect of natural and synthetic fatty acids on membrane structure, microdomain organization, cellular functions and human health. Biochim. Biophys. Acta, Biomembr. 1838 (6), 1518–28.

(106). Meczynska-Wielgosz S, Piotrowska A, Majkowska-Pilip A, Bilewicz A, and Kruszewski M. (2016) Effect of Surface Functionalization on the Cellular Uptake and Toxicity of Nanozeolite A. Nanoscale Res. Lett. 11 (1), 123. [PubMed: 26935303]

(107). Verma NK, Moore E, Blau W, Volkov Y, and Ramesh Babu P. (2012) Cytotoxicity evaluation of nanoclays in human epithelial cell line A549 using high content screening and real-time impedance analysis. J. Nanopart. Res. 14 (9), 1137.

(108). Zhang H, Dunphy DR, Jiang X, Meng H, Sun B, Tarn D, Xue M, Wang X, Lin S, Ji Z, Li R, Garcia FL, Yang J, Kirk ML, Xia T, Zink JI, Nel A, and Brinker CJ (2012) Processing pathway dependence of amorphous silica nanoparticle toxicity: colloidal vs pyrolytic. J. Am. Chem. Soc. 134 (38), 15790–804. [PubMed: 22924492]

(109). Maisanaba S, Pichardo S, Puerto M, Gutierrez-Praena D, Camean AM, and Jos A. (2015) Toxicological evaluation of clay minerals and derived nanocomposites: a review. Environ. Res. 138, 233–54. [PubMed: 25732897]

(110). Han HK, Lee YC, Lee MY, Patil AJ, and Shin HJ (2011) Magnesium and calcium organophyllosilicates: synthesis and in vitro cytotoxicity study. ACS Appl. Mater. Interfaces 3 (7), 2564–72. [PubMed: 21609130]

(111). Zhao F, Zhao Y, Liu Y, Chang X, Chen C, and Zhao Y. (2011) Cellular uptake, intracellular trafficking, and cytotoxicity of nanomaterials. Small 7 (10), 1322–37. [PubMed: 21520409]

(112). Houtman J, Maisanaba S, Puerto M, Gutiérrez-Praena D, Jordá M, Aucejo S, and Jos A. (2014) Toxicity assessment of organomodified clays used in food contact materials on human target cell lines. Appl. Clay Sci. 90, 150–158.

(113). Willhite CC, Karyakina NA, Yokel RA, Yenugadhati N, Wisniewski TM, Arnold IM, Momoli F, and Krewski D. (2014) Systematic review of potential health risks posed by pharmaceutical, occupational and consumer exposures to metallic and nanoscale aluminum, aluminum oxides, aluminum hydroxide and its soluble salts. Crit. Rev. Toxicol. 44, 1–80.

(114). Kondej D, and Sosnowski TR (2013) Alteration of biophysical activity of pulmonary surfactant by aluminosilicate nanoparticles. Inhalation Toxicol. 25 (2), 77–83.

(115). Mousseau F, Le Borgne R, Seyrek E, and Berret JF (2015) Biophysicochemical Interaction of a Clinical Pulmonary Surfactant with Nanoalumina. Langmuir 31 (26), 7346–54. [PubMed: 26075579]

(116). Inácio AS, Costa GN, Domingues NS, Santos MS, Moreno AJM, Vaz WLC, and Vieira OV (2013) Mitochondrial dysfunction is the focus of quaternary ammonium surfactant toxicity to mammalian epithelial cells. Antimicrob. Agents Chemother. 57 (6), 2631–2639. [PubMed: 23529737]

(117). Inacio AS, Domingues NS, Nunes A, Martins PT, Moreno MJ, Estronca LM, Fernandes R, Moreno AJ, Borrego MJ, Gomes JP, Vaz WL, and Vieira OV (2016) Quaternary ammonium surfactant structure determines selective toxicity towards bacteria: mechanisms of action and clinical implications in antibacterial prophylaxis. J. Antimicrob. Chemother. 71 (3), 641–54. [PubMed: 26679255]

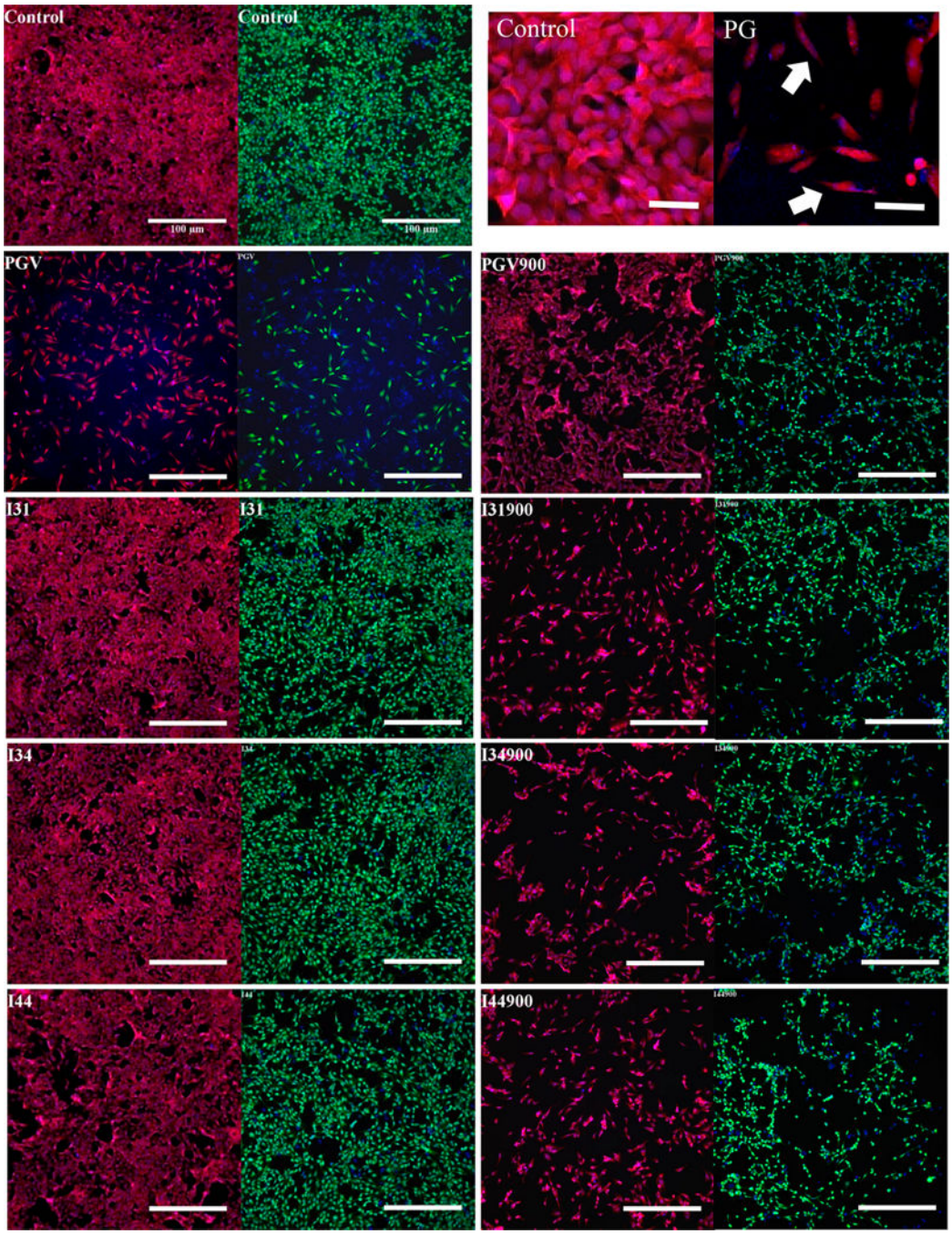

Figure 1.

Representative 10× magnification images from HCI of Nanomer organomodified nanoclay and incinerated byproduct particle exposure to human bronchial epithelial cells monolayer integrity, cell shape, and nuclear morphology. Cell membrane (red) and cytoplasm (green) fluorescent probes were imaged in separate assays with nuclear (blue) probe. Scale bars represent 100 μm. White arrows (upper right panel) indicate cell morphology change from unexposed cuboidal-shaped cells to PGV-exposed elongated cell morphology. Scale bars are 25 μm.

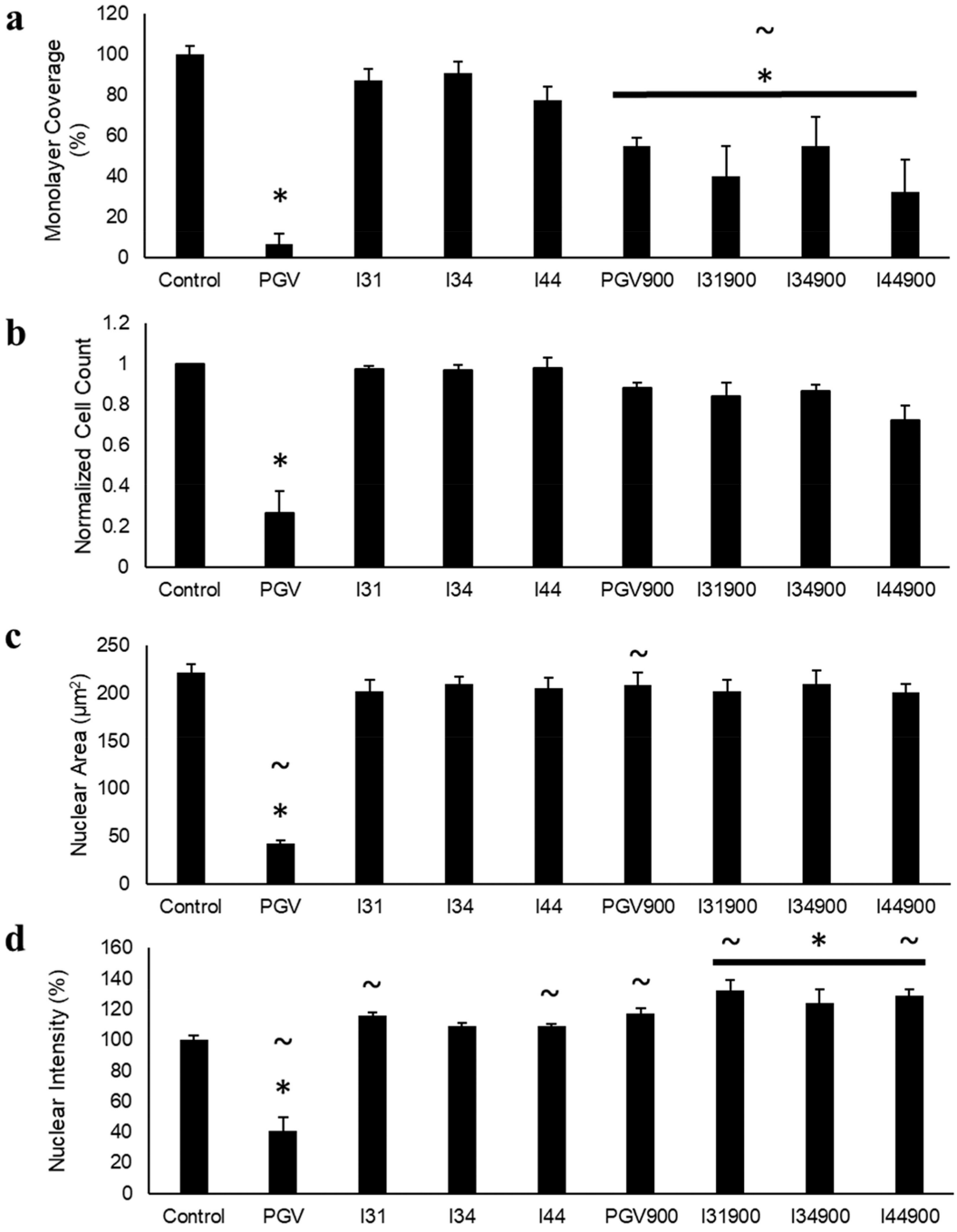

Figure 2.

Quantification of HCI analysis of bronchial epithelial monolayer response to Nanomer organomodified nanoclay and incinerated byproduct exposure: (* and ~) significant differences between the pristine and modified or thermally degraded clays and between nanoclays and their corresponding byproducts, respectively ($p < 0.05$; $n = 8$).

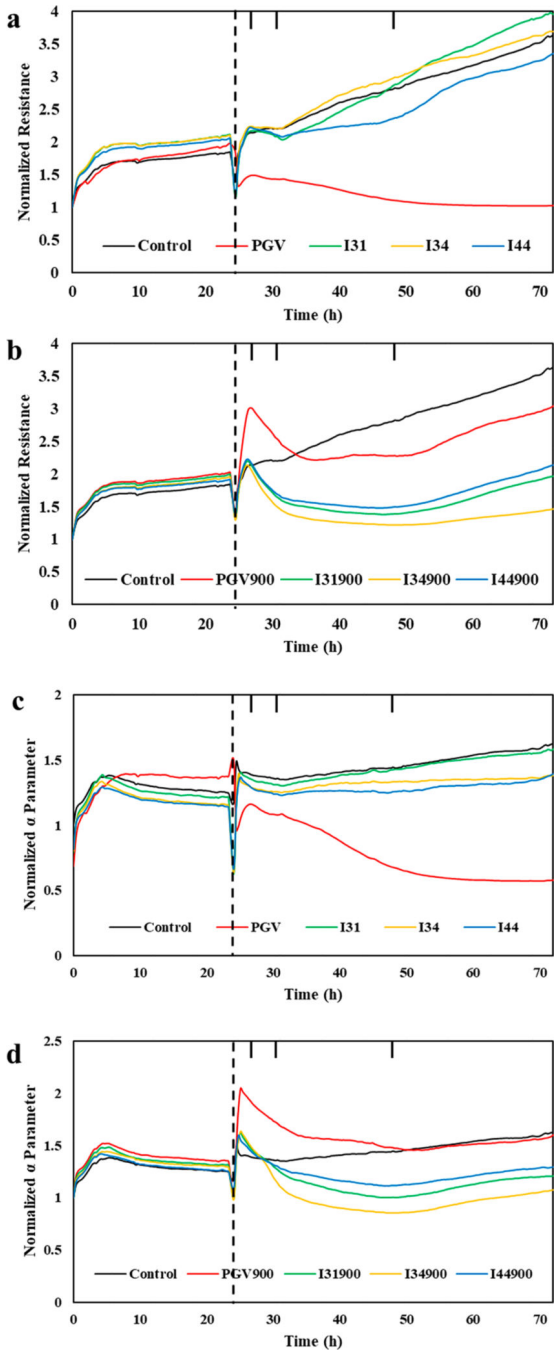

Figure 3.

Representative measurements of normalized resistance upon exposure for 48 h to (a) nanoclays and (b) byproducts. Normalized α parameter is shown for (c) nanoclays and (d) byproducts ($n = 4$). Vertical dashed lines indicate start of particle exposure, while vertical tick marks indicate 2, 7, and 24 h postexposure.

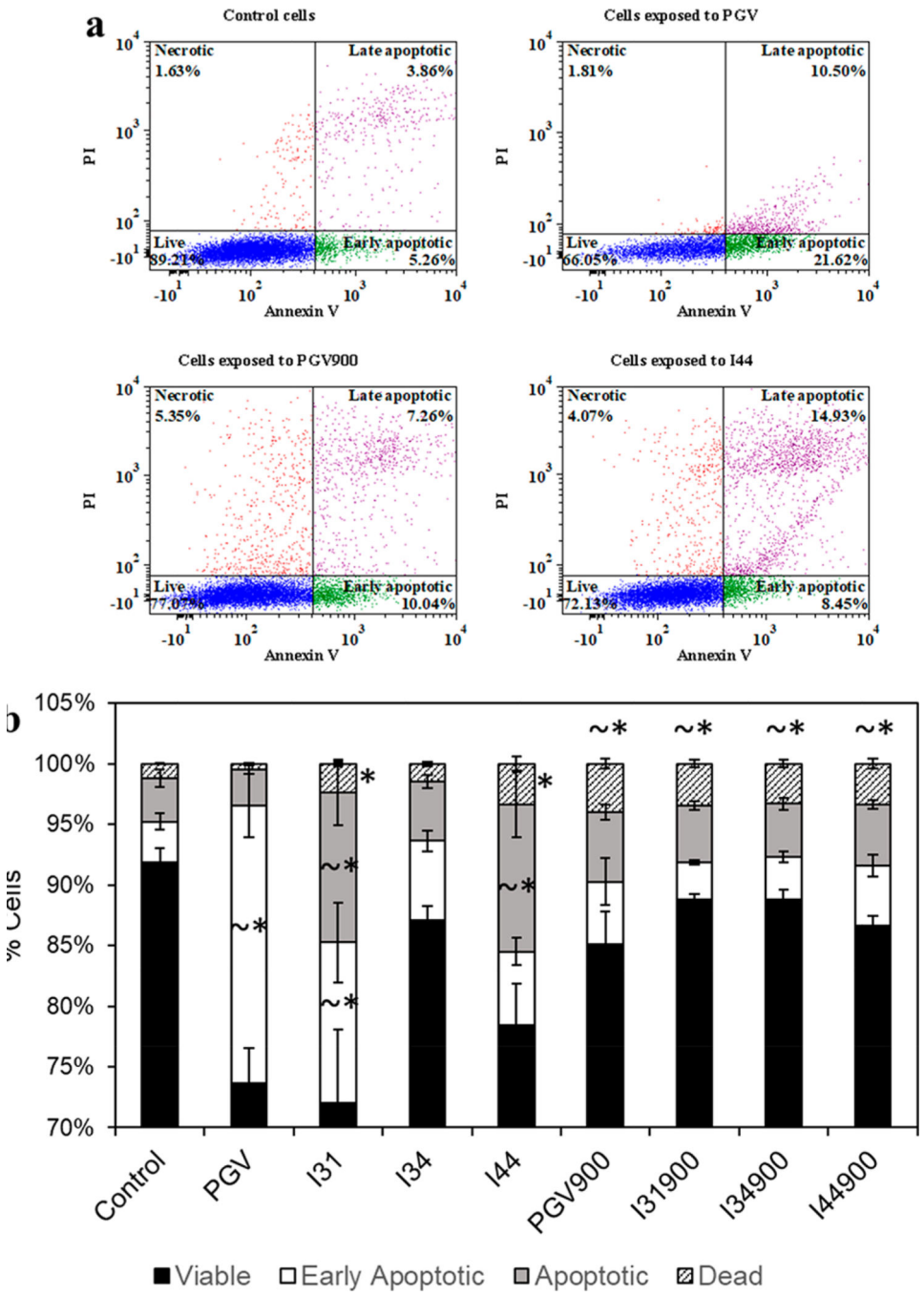

Figure 4.

Flow cytometric analysis of the effect of treatment on cell apoptosis and necrosis. (A) Representative flow cytometry scatter plots. (B) Quantitative comparison of live, apoptotic, and necrotic cells: (*) significant difference between exposed samples and controls; (~) significant difference between nanoclays and the corresponding thermally degraded byproduct ($p < 0.05$; $n = 6$).

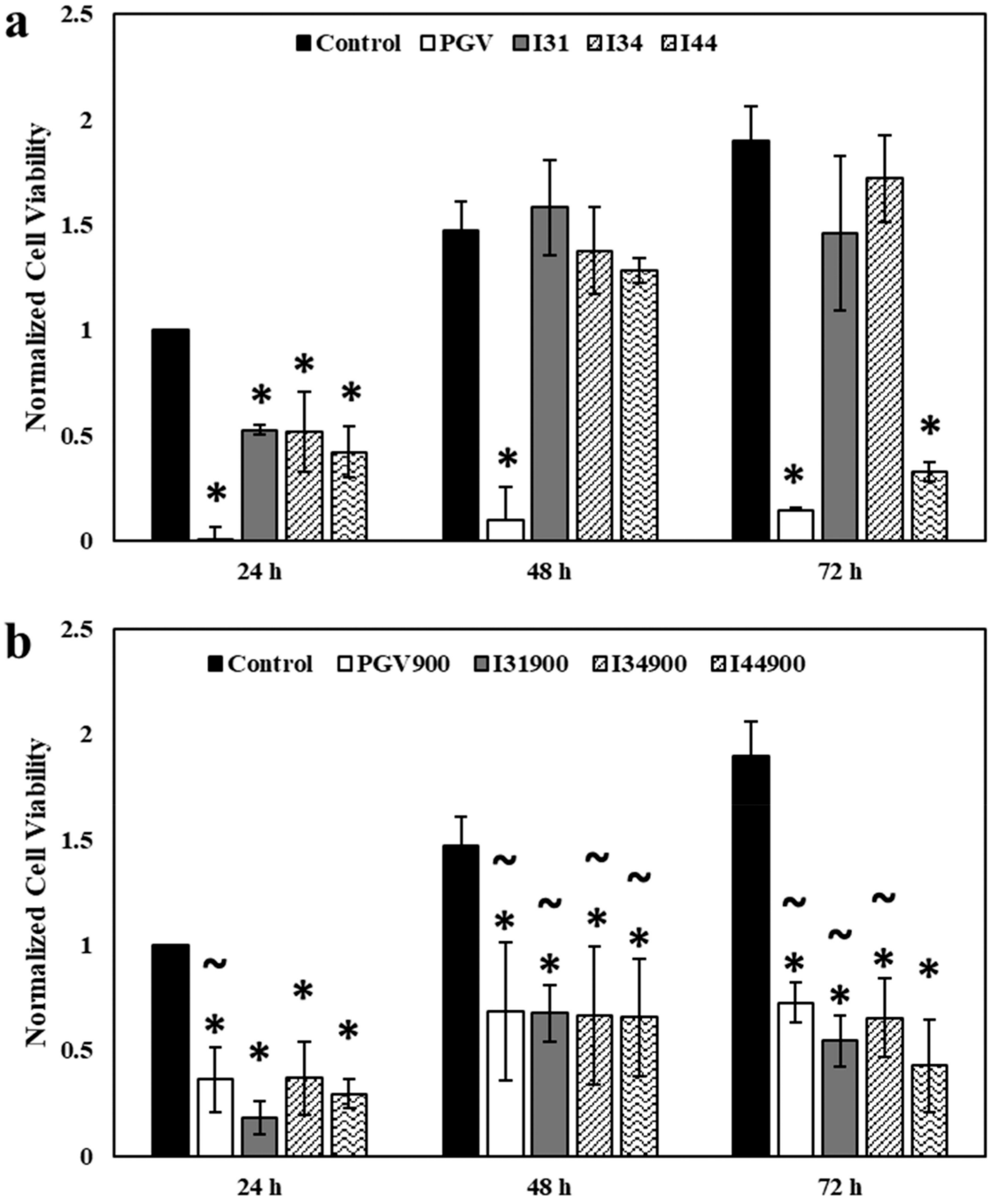

Figure 5.

Cellular viability determined with WST-1 assay after 24, 48, and 72 h exposure to (a) nanoclays and (b) byproducts ($n = 4$): (* and ~) significant differences between the pristine and modified or thermally degraded clays and between nanoclays and their corresponding byproducts, respectively ($p < 0.05$).